Formation of Mixed Spin-state Macrocyclic Dinickel(II) Complexes through Variation of Hole Size†

Kausik K. Nanda,[a] Ramprasad Das,[a] Krishnan Venkatsubramanian,[b] Parimal Paul[b] and Kamalaksha Nag*,[a]

[a] *Department of Inorganic Chemistry, Indian Association for the Cultivation of Science, Calcutta 700 032, India*

[b] *Coordination Chemistry Discipline, Central Salt and Marine Chemicals Research Institute, Bhavnagar 364002, India*

Dinuclear nickel(II) complexes of two tetraaminodiphenol macrocyclic ligands in which one (H_2L^1) has two $-NH(CH_2)_3NH-$ units and the other (H_2L^2) contains one $-NH(CH_2)_3NH-$ and one $-NH(CH_2)_2NH-$ moiety have been studied. In the inclusion complex $[Ni_2L^1(H_2O)_4][ClO_4]_2\cdot4NH_2CONH_2$ **1**, both metal centres are in octahedral configuration. On reaction with pyridine (py), complex **1** transforms into the square-pyramidal complex $[Ni_2L^1(py)_2][ClO_4]_2$. The macrocycle H_2L^2 forms the mixed spin-state complex $[Ni_2L^2(H_2O)_2]I_2$ **2** in which one metal centre is square planar and the other octahedral. On reaction with pyridine, complex **2** produces the square-planar–square-pyramidal complex $[Ni_2L^2(py)]I_2$ **4**; the low-spin Ni^{2+} of both **2** and **4** is accommodated by the smaller N_2O_2 cavity provided by the phenolic oxygens and $-NH(CH_2)_2NH-$ nitrogens. The redox properties of complexes **1** and **2** have been studied by cyclic voltammetry and their crystal structures determined. Complex **1**: $a = 7.530(1)$, $b = 26.499(3)$, $c = 11.434(1)$ Å, $\beta = 96.89(1)°$, $Z = 2$, $R = 0.051$ and $R' = 0.059$. Complex **2**: $a = 11.386(1)$, $b = 20.094(2)$, $c = 13.158(1)$ Å, $\beta = 102.16(1)°$, $Z = 4$, $R = 0.050$, $R' = 0.059$.

The recognition of a metal ion by a macrocyclic ligand and modification of the properties of the resulting complex is controlled to a large extent by a match between the size of the ligand hole and that of the metal ion.[1] Although the size-match selectivity in tetraaza macrocyclic systems have been studied by molecular mechanics calculations,[2-4] a simple procedure has been reported[5,6] to obtain goodness-of-fit for complexes with O_2N_2-, S_2N_2- or N_4-donor sets.

During the course of our studies[7-9] on the dinickel(II) complexes of the tetraaminodiphenol macrocyclic ligand H_2L^1 it became apparent that the cavity produced by the N_2O_2 donors is suitable for high-spin Ni^{2+}. However from a comparison of the Pauling covalent radius of low-spin Ni^{2+} (1.20 Å) and high-spin Ni^{2+} (1.39 Å) it occurred to us that squeezing the macrocycle H_2L^1 by replacing one of its $-NH(CH_2)_3NH-$ moieties with an $-NH(CH_2)_2NH-$ moiety might generate cavities of right sizes to accommodate two nickel atoms under different stereochemical configurations. Juxtaposition of two nickel(II) centres in different spin states, especially with ligands having the same in-plane donor atoms, is of considerable interest because of the rarity of such species[10] and lack of precedence in macrocyclic systems. We report here the structures and reactions of the two complexes, $[Ni_2L^1(H_2O)_4][ClO_4]_2\cdot4NH_2CONH_2$ **1** and $[Ni_2L^2(H_2O)_2]I_2$ **2**, where the metal centres are in octahedral–octahedral and octahedral–square environments.

Results and Discussion

We have reported earlier[7] that the inclusion complex $[Ni_2L^1(MeOH)_2(ClO_4)_2]\cdot2[Et_3NH\cdot ClO_4]$ **3** in methanol exists as $[Ni_2L^1(MeOH)_4]^{2+}$. Although this species gradually changes into $[Ni_2L^1(H_2O)_4]^{2+}$ with the incremental addition of water, isolation of the tetraaqua species in the solid state turned out to be problematic. However, crystals of the inclusion complex **1** were obtained when a methanol solution of **3** was treated with an excess of urea and then allowed to evaporate slowly in air.

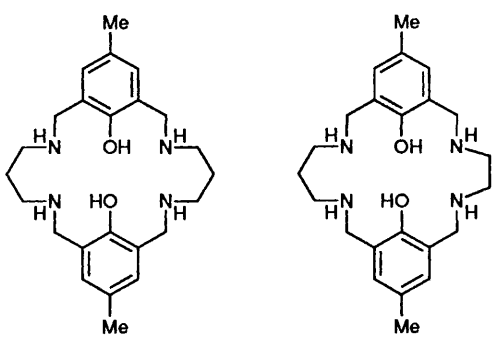

H_2L^1 H_2L^2

The asymmetric macrocycle H_2L^2 was synthesised by the sequential addition of 1 equivalent each of 1,2-diaminoethane (en) and 1,3-diaminopropane (pn) to a boiling methanol solution containing $Mg(NO_3)_2\cdot6H_2O$, $Mg(MeCO_2)_2\cdot4H_2O$ and 2-hydroxy-5-methylbenzene-1,3-dicarbaldehyde (1:1:2) over a period of several hours. After reduction of the di-magnesium Schiff-base macrocyclic complex thus formed with $NaBH_4$, the metal-free H_2L^2 was separated by sequestering magnesium with disodium ethylenediaminetetraacetate. It is important to note that if the order of addition of the diamines is reversed, instead of H_2L^2, solely H_2L^1 is obtained.

Although treatment of $Ni[ClO_4]_2\cdot6H_2O$ (2 equivalents) with a solution of H_2L^2 (1 equivalent) and triethylamine (2 equivalents) gave a deep red solution of $[Ni_2L^2(H_2O)_2]^{2+}$, the perchlorate salt was not amenable to crystallization. Several counter anions were tried but only the iodide salt turned out to afford single crystals.

† *Supplementary data available:* see Instructions for Authors, *J. Chem. Soc., Dalton Trans.*, 1993, Issue 1, pp. xxiii–xxviii.

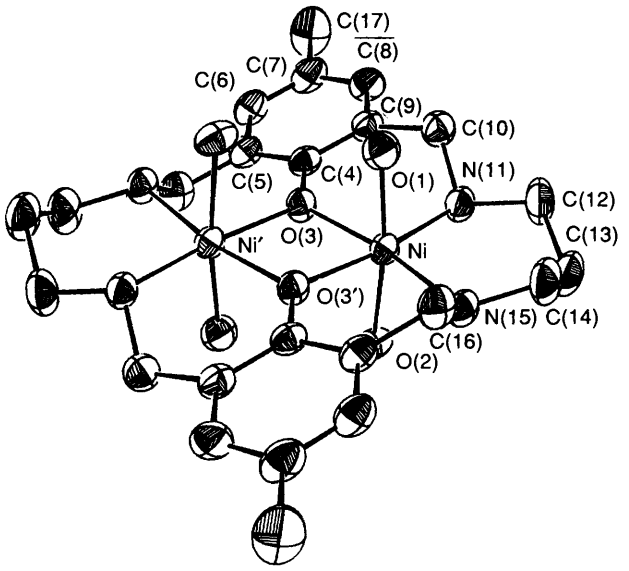

Fig. 1 An ORTEP diagram and atom labelling scheme of the cation $[Ni_2L^1(H_2O)_4]^{2+}$ of **1** showing 50% probability thermal ellipsoids

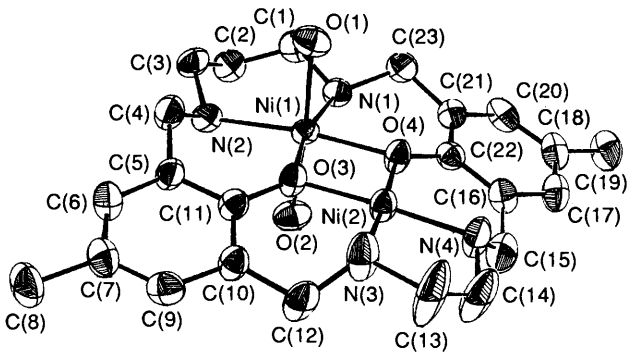

Fig. 2 An ORTEP diagram and atom labelling scheme of the cation $[Ni_2L^2(H_2O)_2]^{2+}$ of **2** showing 50% probability thermal ellipsoids

Characterization.—The IR spectrum of **1** exhibited characteristic bands due to the co-ordinated water (3400 cm^{-1}), urea (3330 and 1650 cm^{-1}) and NH of the macrocyclic ligand (3230 cm^{-1}). A group of highly structured bands observed in the range 1250–1000 cm^{-1} due to $[ClO_4]^-$ provided strong evidence in favour of its involvement in hydrogen bonding. The observation of two NH stretches at 3240 and 3205 cm^{-1} for **2**, as opposed to a single band exhibited by the free ligand at 3260 cm^{-1}, suggested that the two metal centres are not stereochemically equivalent.

The electronic spectrum of **1** in methanol can be interpreted in terms of tetragonally distorted octahedral stereochemistry by relating the five observed bands at 1150, 800, 760, 520 and 370 nm to the transitions from $^3B_{1g}$ to ^3E_g, $^3B_{2g}$, $^3A_{2g}$, ^3E_g and $^3A_{2g}$ and/or $^3E_g(P)$ respectively. Complex **2** in methanol also exhibited these bands at 1200, 800, 740, 465 and 350 nm. A weak shoulder additionally observed at *ca.* 620 nm can be associated to the $^1A_{1g} \longrightarrow {}^1A_{2g}$ transition of square-planar nickel. As will be seen, the UV/VIS spectral characteristics of the two complexes are consistent with their crystal structures. The spectroscopic data of **2** are of special interest because they may be used to estimate the crystal-field splitting parameters[11] of both the square and octahedral nickel centres in the same complex. Thus, while for the octahedral Ni^{2+}, $Dq^{xy} = 1250$ cm^{-1}, for the square Ni^{2+}, $Dq^{xy} = 2100$ cm^{-1}. Considerably stronger in-plane ligand-field strength of the N_2O_2 donors at the square nickel(II) relative to that of the octahedral nickel(II) is not unusual[12,13] because the Ni–N and Ni–O distances at the square nickel are *ca.* 0.15 Å shorter than those of the octahedral nickel.

Table 1 Atomic coordinates with estimated standard deviations (e.s.d.s) in parentheses for $[Ni_2L^1(H_2O)_4][ClO_4]_2 \cdot 4NH_2CONH_2$

Atom	*x*	*y*	*z*
Ni	0.984 39(8)	−0.034 46(2)	1.107 66(5)
Cl(26)	0.475 4(4)	0.200 91(8)	0.595 4(2)
O(1)	0.704 8(5)	−0.033 6(2)	1.056 6(3)
O(2)	1.271 4(5)	−0.025 8(2)	1.147 4(3)
O(3)	1.027 3(5)	−0.039 6(1)	0.936 0(3)
O(18)	0.357 8(6)	0.017 2(2)	0.360 2(3)
O(22)	0.445 6(6)	0.603 4(2)	0.561 8(4)
O(27)	0.481(1)	0.195 2(3)	0.476 6(6)
O(28)	0.604(2)	0.235 5(3)	0.636 1(8)
O(29)	0.506(2)	0.156 5(3)	0.656 2(6)
O(30)	0.310(2)	0.221 5(6)	0.612(1)
N(11)	1.007 3(6)	−0.112 1(2)	1.123 7(3)
N(15)	0.953 8(6)	−0.016 2(2)	1.281 4(3)
N(20)	0.513 4(7)	0.068 1(2)	0.493 5(4)
N(21)	0.351 8(8)	0.101 6(2)	0.329 9(5)
N(24)	0.407(1)	0.686 2(2)	0.582 5(5)
N(25)	0.453 4(8)	0.654 2(2)	0.403 8(5)
C(4)	1.039 6(6)	−0.080 5(2)	0.868 5(4)
C(5)	1.104 3(7)	−0.075 4(2)	0.757 7(4)
C(6)	1.110 5(8)	−0.118 6(2)	0.686 6(4)
C(7)	1.059 9(8)	−0.165 5(2)	0.719 4(5)
C(8)	1.000 5(8)	−0.169 9(2)	0.830 2(5)
C(9)	0.988 9(7)	−0.128 6(2)	0.904 1(4)
C(10)	0.910 0(8)	−0.138 2(2)	1.019 2(5)
C(12)	0.946(1)	−0.135 6(2)	1.230 2(5)
C(13)	1.006(1)	−0.105 6(3)	1.343 2(5)
C(14)	0.895 3(9)	−0.058 8(3)	1.353 4(5)
C(16)	0.825 5(8)	0.026 6(2)	1.284 0(4)
C(17)	1.067(1)	−0.211 0(3)	0.638 5(6)
C(19)	0.403 1(7)	0.060 2(2)	0.393 2(5)
C(23)	0.435 8(8)	0.646 3(2)	0.518 3(6)

Description of the Structures of Complexes **1** *and* **2**.—Perspective views of the complex cations $[Ni_2L^1(H_2O)_4]^{2+}$ and $[Ni_2L^2(H_2O)_2]^{2+}$ are shown in Figs. 1 and 2, respectively along with their atom labelling schemes. For the two compounds atomic coordinates are given in Tables 1 and 2, while selected bond lengths and angles are listed in Tables 3 and 4.

In complex **1** each nickel atom is co-ordinated to two secondary amine nitrogen donors and two bridging phenolate groups from the macrocycle and the tetragonally distorted octahedral geometry is obtained by axial co-ordination of two water molecules. The Ni_2O_2 (phenolate) atoms form an exact plane and there is a centre of inversion at the middle of this plane. The Ni–O distances of the co-ordinated water molecules are unequal [Ni–O(1) 2.116(4), Ni–O(2) 2.167(4) Å] and they are longer relative to the in-plane bonds [Ni–O(3) 2.031(3), Ni–N(11) 2.071(4), Ni–N(15) 2.084(5) Å]. The two metal atoms are separated by 3.100(3) Å, with a Ni–O(3)–Ni' bridge angle of 99.5(1)°. Around nickel the cisoid angles vary between 80.5(2) and 99.4(2)°, whereas the transoid angles lie in the narrow range 170.1(2)–172.3(2)°.

The X-ray crystallography of **2** confirmed that the structure consists of two nickel centres, one octahedral, Ni(1), and the other square planar, Ni(2), bridged by two phenoxide oxygens and the nitrogen donors of the $-NH(CH_2)_3NH-$ and $-NH(CH_2)_2NH-$ units complete the Ni(1)N(1)N(2)O(3)O(4) and Ni(2)N(3)N(4)O(3)O(4) planes, respectively. Atom Ni(1) achieves axially elongated octahedral geometry through the two water molecules. The constituent atoms belonging to the mean plane of Ni(1) lie within 0.01 Å of it, but those of Ni(2) are displaced in the following way: N(3) 0.049, N(4) −0.057, O(3) −0.061, O(4) 0.052, Ni(1) 0.017 Å. Due to the differences in the bite angles of the diamines as well as the O(3)NiO(4) angles, the two metal atoms do not lie exactly on the same plane; the dihedral angle between the two NiN_2O_2 planes is 5.6°. In this compound the distance between the metal centres [2.981(4) Å] is shorter than in **1** [3.100(3)], albeit the NiONi bridging angle

Table 2 Atomic coordinates with estimated standard deviations (e.s.d.s) in parentheses for $[Ni_2L^2(H_2O)_2]I_2$

Atom	x	y	z	Atom	x	y	z
I(1)	0.192 41(9)	0.145 37(5)	0.759 97(7)	C(7)	0.554(1)	0.045 1(6)	0.119(1)
I(2)	0.666 01(8)	0.154 09(5)	0.686 46(7)	C(8)	0.484(1)	−0.007 7(7)	0.164(1)
Ni(1)	0.929 3(1)	0.201 39(7)	0.024 2(1)	C(9)	0.501(1)	0.100 1(6)	0.070 4(9)
Ni(2)	0.697 1(1)	0.257 81(7)	−0.091 0(1)	C(10)	0.564 0(9)	0.148 8(6)	0.026 2(9)
O(1)	0.941 4(7)	0.141 6(4)	−0.110 2(6)	C(11)	0.686 8(9)	0.138 5(5)	0.030 7(8)
O(2)	0.911 8(7)	0.254 0(4)	0.161 9(6)	C(12)	0.499(1)	0.208 8(7)	−0.022(1)
O(3)	0.751 6(6)	0.182 8(4)	−0.012 2(6)	C(13)	0.461(1)	0.286 0(8)	−0.172(2)
O(4)	0.859 7(6)	0.278 0(4)	−0.068 6(6)	C(14)	0.516(1)	0.342 8(8)	−0.167(2)
N(1)	1.099 2(8)	0.239 8(5)	0.043 1(7)	C(15)	0.712(1)	0.395 5(7)	−0.115(1)
N(2)	0.960 2(7)	0.117 1(5)	0.114 2(7)	C(16)	0.845(1)	0.393 2(6)	−0.114 7(9)
N(3)	0.534 2(8)	0.231 5(6)	−0.114 5(9)	C(17)	0.901(1)	0.452 1(6)	−0.133(1)
N(4)	0.646 5(8)	0.339 1(5)	−0.160 6(8)	C(18)	1.025(1)	0.456 4(6)	−0.121 3(9)
C(1)	1.197(1)	0.190 3(7)	0.072(1)	C(19)	1.085(1)	0.520 7(6)	−0.137(1)
C(2)	1.179(1)	0.143 9(7)	0.157 8(9)	C(20)	1.090(1)	0.400 0(6)	−0.089 5(9)
C(3)	1.085(1)	0.090 8(6)	0.124(1)	C(21)	1.036(1)	0.339 1(5)	−0.073 4(8)
C(4)	0.872(1)	0.064 6(6)	0.078(1)	C(22)	0.911 1(9)	0.336 1(5)	−0.085 4(8)
C(5)	0.745(1)	0.081 8(5)	0.080 9(9)	C(23)	1.115(1)	0.278 8(6)	−0.050 0(9)
C(6)	0.676(1)	0.037 2(6)	0.124 5(9)				

Table 3 Selected bond distances (Å) and angles (°) for $[Ni_2L^1(H_2O)_4][ClO_4]_2{\cdot}4NH_2CONH_2$ **1**

Ni–O(1)	2.116(4)	Ni–O(3′)	2.031(3)
Ni–O(2)	2.167(4)	Ni–N(11)	2.071(4)
Ni–O(3)	2.031(3)	Ni–N(15)	2.084(5)
Ni · · · Ni′	3.100(3)		
O(1)–Ni–O(2)	172.3(2)	O(2)–Ni–N(15)	89.9(1)
O(1)–Ni–O(3)	90.1(1)	O(3)–Ni–O(3′)	80.5(2)
O(1)–Ni–O(3′)	84.8(1)	O(3)–Ni–N(11)	89.9(1)
O(1)–Ni–N(11)	96.0(2)	O(3)–Ni–N(15)	170.1(2)
O(1)–Ni–N(15)	92.4(2)	O(3′)–Ni–N(11)	170.3(1)
O(2)–Ni–O(3)	86.5(1)	O(3′)–Ni–N(15)	90.2(2)
O(2)–Ni–O(3′)	87.8(1)	N(11)–Ni–N(15)	99.4(2)
O(2)–Ni–N(11)	90.9(2)	Ni–O(3)–Ni′	99.5(1)

Table 4 Selected bond distances (Å) and angles (°) for $[Ni_2L^2(H_2O)_2]I_2$ **2**

Ni(1)–O(1)	2.167(8)	Ni(2)–O(3)	1.859(7)
Ni(1)–O(2)	2.143(8)	Ni(2)–O(4)	1.859(7)
Ni(1)–O(3)	2.014(7)	Ni(2)–N(3)	1.90(1)
Ni(1)–O(4)	2.020(7)	Ni(2)–N(4)	1.90(1)
Ni(1)–N(1)	2.049(9)	Ni(1) · · · Ni(2)	2.981(4)
Ni(1)–N(2)	2.054(9)		
O(1)–Ni(1)–O(2)	175.6(3)	O(4)–Ni(1)–N(1)	91.5(3)
O(1)–Ni(1)–O(3)	86.3(3)	O(4)–Ni(1)–N(2)	167.0(4)
O(1)–Ni(1)–O(4)	90.8(4)	N(1)–Ni(1)–N(2)	101.4(3)
O(1)–N(1)–N(1)	95.0(3)	O(3)–Ni(2)–O(4)	83.4(4)
O(1)–Ni(1)–N(2)	88.9(3)	O(3)–Ni(2)–N(3)	93.7(4)
O(2)–Ni(1)–O(3)	91.4(3)	O(3)–Ni(2)–N(4)	174.9(4)
O(2)–Ni(1)–O(4)	92.3(3)	O(4)–Ni(2)–N(3)	176.4(4)
O(2)–Ni(1)–N(1)	88.0(4)	O(4)–Ni(2)–N(4)	94.6(4)
O(2)–Ni(1)–N(2)	87.4(3)	N(3)–Ni(2)–N(4)	88.6(4)
O(3)–Ni(1)–O(4)	75.5(3)	Ni(1)–O(3)–Ni(2)	100.6(3)
O(3)–Ni(1)–N(1)	167.0(3)	Ni(1)–O(4)–Ni(2)	100.4(3)
O(3)–Ni(1)–N(2)	91.5(3)		

[100.5(3)°] does not differ significantly from that of **1**. A comparison of the Ni–N and Ni–O bond lengths in the equatorial planes of **2** reveals that the bonds involving the square-planar nickel(II) are *ca.* 0.15 Å shorter than the bonds to the octahedral nickel(II).

The packing diagrams of complexes **1** and **2** are shown in Figs. 3 and 4, respectively. The iodine atoms in the unit cell of **2** are located more than 3.5 Å away from the nearest water molecules or NH groups and therefore are not involved in hydrogen bonding. On the other hand there is an extensive network of hydrogen bonding in **1** involving NH_2CONH_2, ClO_4^-, NH of the macrocycle and the water molecules. Table 5 lists ten such D–H · · · A (D = donor, A = acceptor) distances which are less than 3.2 Å and the symmetry relations between the donors and acceptors.

The goodness-of-fit of the two metal centres in the N_2O_2 cavities of **2** was estimated by comparing r_A to r_P ratios[5,6] where r_A is the bonding cavity available in the metal-binding site and r_P is the Pauling covalent radius of the metal ion. For the octahedral site, the diameter of the macrocyclic hole d_m is 4.05 Å which gives[5,6] r_A = 1.37 Å. Since for octahedral Ni^{2+}, r_P is 1.39 Å, r_A/r_P = 0.985 indicates a quite good fit of Ni^{2+} in the cavity. For the square-planar site (d_m 3.75 Å, r_A = 1.205 Å, r_P = 1.20 Å) again the metal ion shows a very good size-match relationship. It should be noted that the diameter of the macrocyclic hole in **2** (4.10 Å) is ideally suited for octahedral nickel.

The co-ordination environments of the two nickel atoms in complex **2** explain the magnetic properties of the complex. The temperature independent susceptibility of the compound (μ_{eff} = 3.18 at 300 K and 3.0 at 80 K) is consistent with S = 0 and S = 1 spin states of the two nickel sites.

Equilibrium Constants.—We have earlier demonstrated[8] that complex **3** on treatment with monodentate nitrogen donors (B) gives square-pyramidal $[Ni_2L^1(B)_2][ClO_4]_2$ complexes and have reported the structure of the pyridine derivative. It was our interest, therefore, to see the change in the co-ordination spheres of **2** on reaction with pyridine (py). Addition of a large excess of pyridine to **2** afforded a green complex of composition $[Ni_2L^2(py)]I_2$ **4**. Complex **4** similarly to **2** exhibited two NH frequencies at 3240 and 3200 cm^{-1}, and its room-temperature magnetic moment was 3.26. The electronic spectra of **2** and **4** in py–MeOH (1 : 1) were identical and the bands observed at 1450, 890, 840, 750, 600 and 375 may be tentatively assigned to the transitions from the $^3B_1$ ground state to $^3E(F)$, $^3B_2(F)$, $^3A_2(F)$, $^3E(F)$, $^3E(P)$ and $^3A_2(P)$ levels in high-spin square-pyramidal nickel(II). Interestingly, **4** slowly changes to **2** when left exposed to air for a long time.

Fig. 5 shows changes in the UV/VIS spectrum of **2** at various concentrations of pyridine in methanol. It may be noted that the band at 465 nm due to the octahedral nickel gradually disappeared at the expense of the band evolved at 600 nm due to the square-pyramidal nickel. Analysis of the spectrophotometric data[14] showed the presence of only two light absorbing species in solution, which clearly indicated that the stereochemistry of the square-planar nickel remained unchanged. The equilibrium constant (K_1) determined[15] for equilibrium (1) was

Table 5 Inter- and intra-molecular hydrogen-bond distances (Å) and angles (°) for $[Ni_2L^1(H_2O)_4][ClO_4]_2 \cdot 4NH_2CONH_2$

D	H	A	D···A	D–H···A	Symmetry
O(1)	H(11)	O(22)[a]	2.696	172.2	$2 - x, \frac{1}{2} + y, \frac{1}{2} - z$
O(1)	H(12)	O(2)	2.836	153.7	$1 - x, -y, 1 - z$
O(2)	H(21)	O(22)[a]	2.688	170.8	$1 - x, \frac{1}{2} + y, \frac{1}{2} - z$
O(2)	H(21)	O(18)[a]	2.695	156.8	$1 - x, -y, 1 - z$
N(11)	H(111)	O(22)[a]	3.021	100.3	x, y, z
N(15)	H(151)	O(18)	3.193	175.7	$1 + x, y, 1 + z$
N(20)[a]	H(201)	O(18)[a]	2.907	162.5	$1 - x, y, 1 - z$
N(20)[a]	H(202)	O(29)[b]	2.996	159.1	x, y, z
N(21)[a]	H(212)	O(27)[b]	3.089	162.9	x, y, z
N(25)[a]	H(252)	O(28)[b]	2.983	159.0	$1 - x, 1 - y, 1 - z$

[a] NH_2CONH_2. [b] ClO_4^-

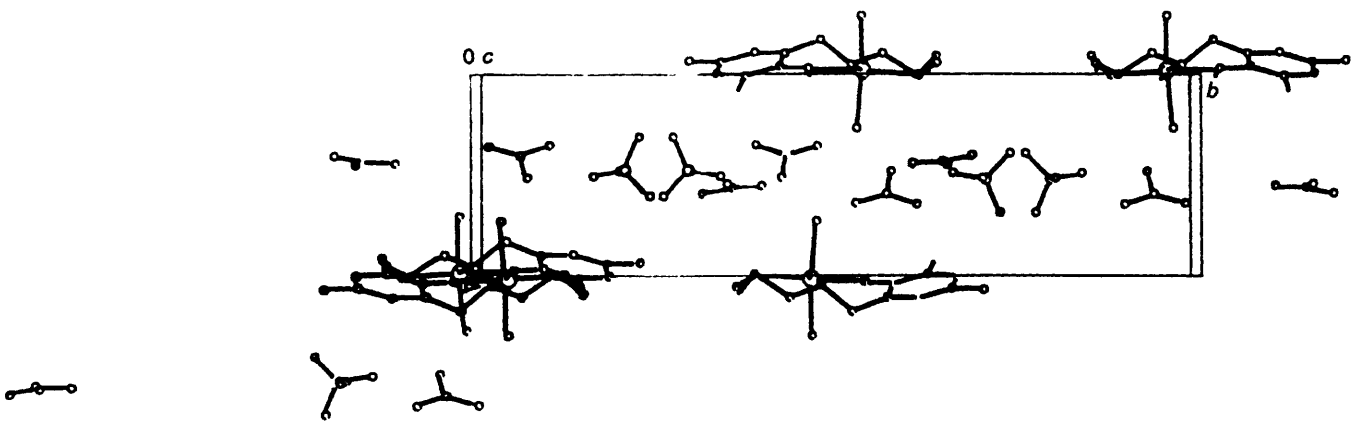

Fig. 3 Packing diagram of $[Ni_2L^1(H_2O)_4][ClO_4]_2 \cdot 4NH_2CONH_2$ **1** in the unit cell

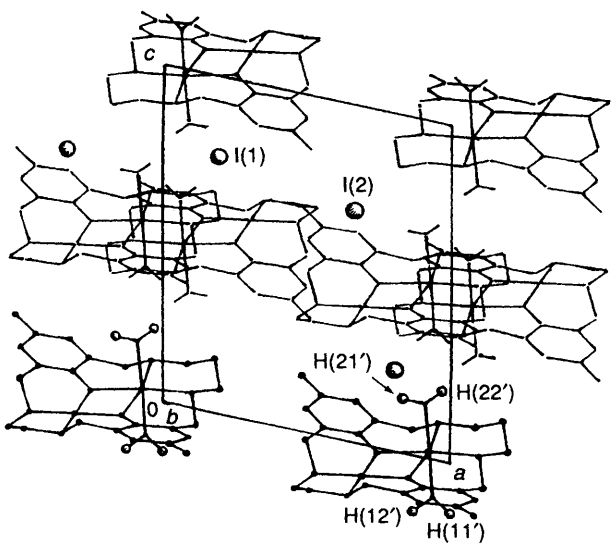

Fig. 4 Packing diagram of $[Ni_2L^2(H_2O)_2]I_2$ **2** in the unit cell

$$[Ni_2L^2(H_2O)_2]^{2+} + py \rightleftharpoons [Ni_2L^2(py)]^{2+} + 2H_2O \quad (1)$$

found to be = 0.8 ± 0.1 $dm^3\ mol^{-1}$. For the sake of comparison the binding constant for a molecule of py to a single metal centre in **1** [equilibrium (2)] was also determined, K_1 = 12.0 ±

$$[Ni_2L^1(H_2O)_4]^{2+} + 2py \rightleftharpoons [Ni_2L^1(py)_2]^{2+} + 4H_2O \quad (2)$$

0.1 $dm^3\ mol^{-1}$ (the overall equilibrium constant $\beta_2 = K_1^2/2$ = 72 $dm^6\ mol^{-2}$. The fifteen-fold increase in the value of K_1 for **1** relative to that of **2** might appear quite surprising. This anomaly, however, becomes clear when steric strains associated with the formation of $[Ni_2L^2(py)]^{2+}$ *vis-a-vis* $[Ni_2L^1(py)_2]^{2+}$ are considered. $[Ni_2L^1(py)_2][ClO_4]_2$ has a centrosymmetric structure[8] and the two square-pyramidal metal centres are displaced in the opposite direction from the equatorial plane by 0.33 Å. However, in the case of **4** only one metal is displaced from the mean plane and this produces considerable strain in the molecule. Thus, while ligand-field effects favour the forward reaction in equilibrium (1), steric constraints act in the opposing direction. The low K_1 value for equilibrium (1) also explains the solid-state transformation of **4** to **2**. The fact that the size of the hole, N_2O_2, bearing the $-NH(CH_2)_3NH-$ moiety is not compatible with the size of low-spin Ni^{2+} explains why neither **2** nor **4** can be converted to a diamagnetic square–square species.

Electrochemistry.—The cyclic voltammogram of complex **1** in MeCN (Pt electrode) in the positive potential range (Fig. 6) exhibits two metal-centred reversible one-electron oxidation steps [$^1E_{\frac{1}{2}}$ = 0.95 V, $^2E_{\frac{1}{2}}$ = 1.10 V *vs.* saturated calomel electrode (SCE)]. For both Ni^{II}–Ni^{III} and Ni^{III}–Ni^{III} redox couples the separation of peak potentials ($E_{pa} - E_{pc}$ = 70 ± 10 mV), the ratio i_{pa}/i_{pc} and $i_{pa}v^{\frac{1}{2}}$ remained practically constant when the scan rate v was varied between 50 and 500 mV s^{-1}. Differential pulse voltammetric measurements also revealed the occurrence of two waves with the same pulse heights at the indicated potentials. Reduction of the two metal centres of complex **1** (to $Ni^{I}N^{II}$ and $Ni^{I}Ni^{I}$) occurred irreversibly (MeCN, Pt) at −0.8 and −1.2 V *vs.* SCE.

Fig. 7 shows the redox behaviour of complex **2** and $[Ni_2L^2(H_2O)_2]^{2+}$ (generated by treating **2** with $Ag[ClO_4]$) in MeCN (Pt electrode) in the positive potential range. It may be noted that up to 1.7 V, $[Ni_2L^2(H_2O)_2]^{2+}$ exhibits a single irreversible wave at 1.16 V which must be metal-centred. This wave is seen at the same potential also for **2**, but in this case two more quasireversible oxidation processes are observed with $E_{\frac{1}{2}}$ = 0.61 and 0.44 V. Clearly, these two couples are associated with the electron transfer process $I^- \rightleftharpoons \frac{1}{2}I_2 + e^-$. While the couple at 0.61 V is certainly due to the diffusion controlled

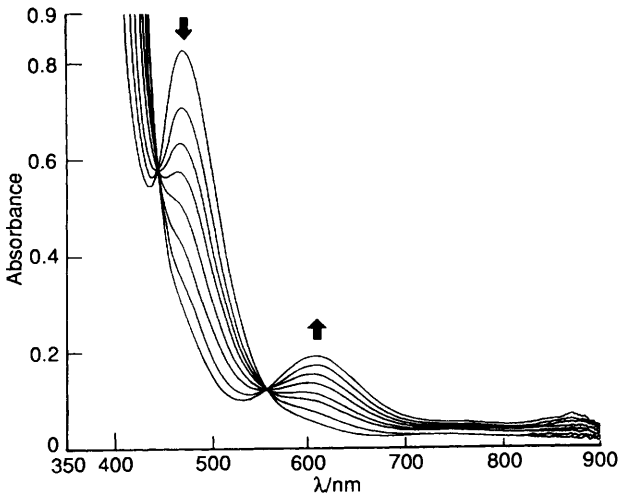

Fig. 5 Visible spectral changes of $[Ni_2L^2(H_2O)_2]I_2$ **2** (5.252×10^{-3} mol dm^{-3}) in MeOH upon addition of varying amounts of pyridine (0–10 mol dm^{-3}). The arrow indicates the increase in concentration of $[Ni_2L^2(py)]^{2+}$

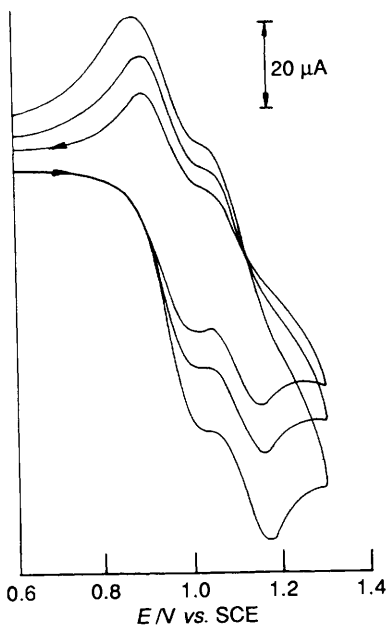

Fig. 6 Cyclic voltammogram of complex **1** in MeCN with a Pt electrode at scan rates of 50, 100 and 200 mV s^{-1}

process, the one at 0.44 V seems to be due to an adsorption phenomenon. This conclusion received support from the fact that, as expected, for strongly adsorbed product, $(i_p)_{ads}$ increased linearly with ν,[16] while $(i_p)_{diff}$ varied linearly with $\nu^{\frac{1}{2}}$. The free energy of adsorption of iodine makes the oxidation of iodide to adsorbed iodine easier than to free iodine in solution. Concerning oxidation at the metal centres, by analogy with complex **1** only the octahedral nickel(II) was oxidized. The reduction of the two metal centres took place irreversibly at −1.3 and −1.6 V.

Experimental

Materials.—All chemicals were reagent grade and used as received. The solvents were dried by standard procedures. 2-Hydroxy-5-methylbenzene-1,3-dicarbaldehyde,[17] H_2L^1 (ref. 18) and $[Ni_2L^1(MeOH)_2(ClO_4)_2]\cdot 2[Et_3NH\cdot ClO_4]$[7] **3** were prepared according to the reported methods.

Syntheses.—H_2L^2. To a boiling MeOH solution (100 cm^3) of $Mg(NO_3)_2\cdot 6H_2O$ (1.28 g, 5 mmol), $Mg(MeCO_2)_2\cdot 4H_2O$ (1.07

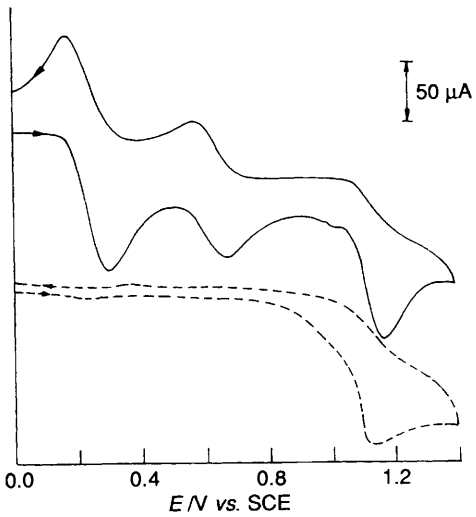

Fig. 7 Cyclic voltammogram of complex **2** in MeCN with a Pt electrode at a scan rate of 50 mV s^{-1}. The broken line (– – – –) shows the voltammogram of $[Ni_2L^2(H_2O)_2]^{2+}$ generated by treating **2** with $Ag[ClO_4]$

g, 5 mmol) and 2-hydroxy-5-methylbenzene-1,3-dicarbaldehyde (1.64 g, 10 mmol) was added a solution (50 cm^3) of 1,2-diaminoethane (0.3 g, 5 mmol) over a period of 2 h. After additional reflux for 1 h, a second MeOH solution (50 cm^3) of 1,3-diaminopropane (0.37 g, 5 mmol) was similarly added. The solution was refluxed for a total of 10 h and then concentrated on a rotary evaporator to deposit orange-red crystals of the dimagnesium Schiff-base macrocyclic complex. This was filtered off and air dried; yield 2 g. The magnesium complex in MeOH (50 cm^3) under stirring was slowly treated with solid $NaBH_4$ (1.5 g). When the mixture became almost colourless it was poured into water (500 cm^3) and made slightly acidic with HCl (6 mol dm^{-3}). The solution was treated with 10 g of disodium ethylenediaminetetraacetate and enough NH_3 to bring the pH to 10. An off-white solid separated which was extracted with $CHCl_3$ (3 × 50 cm^3). The $CHCl_3$ layer was washed with water and dried over Na_2SO_4. After complete removal of the solvent a pale yellow solid was obtained, which was extracted with light petroleum (b.p. 80–100 °C) in a Soxhlet apparatus. The product on further recrystallization from light petroleum gave white crystals, m.p. 150–151 °C; yield 1 g (50%) (Found: C, 69.2; H, 8.65; N, 14.15. $C_{23}H_{34}N_4O_2$ requires C, 69.35; H, 8.55; N, 14.05%). $\tilde{\nu}/cm^{-1}$ 3260 [ν(NH)] and 1610 [δ(NH)]; δ_H 1.74 (2 H, m, $CH_2CH_2CH_2$), 2.20 (6 H, s, Me), 2.70 (4 H, t, $CH_2CH_2CH_2$), 2.81 (4 H, s, CH_2CH_2) 3.79, 3.83 (8 H, s, aryl-CH_2), 6.77 (4 H, s, aryl H); δ_C 20.3 (Me), 29.7 ($CH_2CH_2CH_2$), 47.4 ($CH_2CH_2CH_2$), 48.4 (CH_2CH_2), 51.3 (aryl-CH_2), 124.3, 124.5, 127.4, 128.9, 154.2 (aryl C).

$[Ni_2L^1(H_2O)_4][ClO_4]_2\cdot 4NH_2CONH_2$ **1**. To a MeOH solution (30 cm^3) of complex **3** (1.2 g, 1 mmol), urea (0.4 g) was added. Over a few hours the wine-red solution turned olive green, and was allowed to evaporate slowly in air. After 40 h the sky-blue crystals that deposited were collected by filtration and washed with a few drops of cold MeOH (Found: C, 32.65; H, 5.75; N, 16.3; Ni, 11.4. $C_{28}H_{58}Cl_2N_{12}Ni_2O_{18}$ requires C, 32.35; H, 5.6; N, 16.2; Ni, 11.3%). $\tilde{\nu}/cm^{-1}$ 3400 [ν(OH)], 3330, 3230 [ν(NH)], 1650 [ν(CO)], 1610 [δ(NH)], 1215, 1140, 1110, 1090, 1030 and 630 [ν(ClO_4^-)]; $\lambda_{max}/nm(\varepsilon/dm^3\ mol^{-1}\ cm^{-1})$ (MeOH) 1150(9), 800(6), 760(6), 520(90), 370(520) and 292(7000).

$[Ni_2L^2(H_2O)_2]I_2$ **2**. To a boiling MeOH solution (50 cm^3) containing H_2L^2 (0.8 g, 2 mmol) and triethylamine (0.4 g, 4 mmol) a solution of $Ni[ClO_4]_2\cdot 6H_2O$ (1.46 g, 4 mmol) in MeOH (5 cm^3) was added. The red solution was refluxed for 1 h and then concentrated (*ca.* 20 cm^3) on a rotary evaporator. The solution was cooled and to it an aqueous solution (10 cm^3) of KI (2 g) was added with stirring. The pink compound deposited

was filtered off and recrystallized from hot water (Found: C, 34.15; H, 4.55; N, 6.85; Ni, 14.7. $C_{23}H_{36}I_2N_4Ni_2O_4$ requires C, 34.35; H, 4.5; N, 6.95; Ni, 14.6%). $\tilde{\nu}$/cm^{-1} 3350 [ν(OH)], 3240, 3205 [ν(NH)] and 1600 [δ(NH)]; λ_{max}/nm(ε/dm^3 mol^{-1} cm^{-1}) 1200(7), 800(6), 740(7), 620(sh), 465(165), 350(600) and 295(1680).

$[Ni_2L^2(py)]I_2$ **4**. On diffusion of Et_2O into a MeOH–py (1:1) solution of **2** deep green crystals of **4** deposited. The product was filtered off and washed several times with dry Et_2O (Found: C, 40.2; H, 4.5; N, 8.45; Ni, 13.65. $C_{28}H_{37}I_2N_5Ni_2O_2$ requires C, 39.7; H, 4.35; N, 8.25; Ni, 13.9%). $\tilde{\nu}$/cm^{-1} 3240, 3200 [ν(NH)] and 1600 [δ(NH)]: λ_{max}/nm(ε/dm^3 mol^{-1} cm^{-1}) [MeOH–py (1:1)] 1450(25), 890(14), 840(14), 750(13), 600(45), 375(1300) and 290(1770).

Physical Measurements.—Proton and ^{13}C NMR spectra were recorded on a Bruker WH270 spectrometer. The spectra were obtained as $CDCl_3$ solutions using $SiMe_4$ (δ = 0) as the internal reference. Infrared spectra were recorded on a Perkin Elmer 783 spectrophotometer using KBr discs, electronic spectra on a Shimadzu UV-160A or Hitachi U3400 spectrophotometer in the UV/VIS and near-IR regions. Magnetic susceptibilities were measured on an EG & G PAR 155 vibrating sample magnetometer using $[HgCo(NCS)_4]$ as the calibrant. Electrochemical data were obtained with a BAS100B electrochemistry system. A three electrode assembly (BAS) comprising of a Pt working electrode, a Pt auxiliary electrode and a saturated calomel reference electrode was used. Tetramethylammonium perchlorate (0.1 mol dm^{-3}) was used as the supporting electrolyte. The C, H and N analyses were performed on a Perkin Elmer 240C elemental analyser. Nickel was estimated gravimetrically as dimethylglyoximate.

Equilibrium Constants.—The equilibrium constants for reactions (1) and (2) were determined spectrophotometrically at 25 ± 0.5 °C by recording a series of spectra of methanol solutions of complex **1** or **2** mixed with varying quantities of pyridine. The concentration of the complexes were held fixed between 5 and 6 mmol dm^{-3}, and that of pyridine varied till no further change in the absorbance was noted.

Crystal Structure Determination of $[Ni_2L^1(H_2O)_4][ClO_4]_2 \cdot 4NH_2CONH_2$ **1** *and* $[Ni_2L^2(H_2O)_2]I_2$ **2**.—Both crystals were air stable, in each case a suitable crystal was mounted on a glass fibre.

Crystal data for **1**. $C_{28}H_{58}Cl_2N_{12}Ni_2O_{18}$, M = 1039.1, monoclinic, space group $P2_1/c$, a = 7.530(1), b = 26.499(3), c = 11.434(1) Å, β = 96.89(1)°, U = 2265(1) Å^3 (by least-squares fit of 25 arbitrarily chosen higher-order reflections, λ = 0.710 69 Å), Z = 2, D_c = 1.316 g cm^{-3}, crystal dimensions 0.21 × 0.18 × 0.15 mm, μ(Mo-K$_\alpha$) 10.32 cm^{-1}.

Crystal data for **2**. $C_{23}H_{36}I_2N_4Ni_2O_4$, M = 803.8, monoclinic, space group $P2_1/c$, a = 11.386(1), b = 20.094(2), c = 13.158(1) Å, β = 102.16(1)°, U = 2942.7(7) Å^3 (by least-squares fit of 25 arbitrarily chosen higher-order reflections, λ = 0.710 68 Å), Z = 4, D_c = 1.814 g cm^{-3}, crystal dimensions 0.32 × 0.18 × 0.12 mm, μ(Mo-Kα) 33.954 cm^{-1}.

Data collection and processing. Intensity data were collected for both crystals with an Enraf–Nonius CAD4 diffractometer at 293 K using graphite-monochromated Mo-Kα radiation. Crystal stabilities were checked by monitoring intensities of three standard reflections after every 100 and no significant variations were observed. The intensity data were corrected for Lorentz-polarization effects and for absorption by the empirical method of North *et al.*[19] For complex **1** a total of 4434 reflections were collected in the range 2 < 2θ < 48°, of which 3333 reflections with $I > 3\sigma(I)$ were used for structure determination. For **2** the total number of reflections measured were 4351 (2θ range 2–47°), of which 3307 with $I > 3\sigma(I)$ were considered observed and used in the structure analysis.

Structure analysis and refinement. The structures of both complexes **1** and **2** were solved by direct and Fourier difference methods using the program MULTAN 82.[20] Hydrogen atoms were generated either using stereochemical constraints or located in the difference Fourier map after complete convergence of the anisotropic refinement and were given 1.3 times the thermal parameter of the atoms to which they are bonded. The structures were refined by block-diagonal least-squares techniques. The refinement of **1** converged to R = 0.051, R' = 0.059; for **2**, the corresponding values were R = 0.050, R' = 0.059. Unit-weighting schemes with a Dunitz–Seiler factor[21] were used in the final stages of the refinements. The final difference map for **1** showed ripples of 0.33 e Å^{-3} around the heavy atoms, while for **2** peaks were seen around Ni (0.85 e Å^{-3}) and I (1.32 e Å^{-3}). The scattering factors were taken from ref. 22. All computations were carried out using the structure determination package[23] available with Enraf–Nonius PDP-11/73. Drawings of the structures were generated with the ORTEP program.[24]

Additional material available from the Cambridge Crystallographic Data Centre comprises H-atom coordinates, thermal parameters and remaining bond lengths and angles.

Acknowledgements

K. N. thanks the Science and Engineering Research Council, Department of Science and Technology, Government of India, New Delhi for supporting this research programme.

References

1 L. F. Lindoy, *The Chemistry of Macrocyclic Ligand Complexes*, Cambridge University Press, Cambridge, 1989.
2 D. H. Busch, *Acc. Chem. Res.*, 1978, **11**, 393.
3 R. D. Hancock and G. J. McDougall, *J. Am. Chem. Soc.*, 1980, **102**, 6551.
4 R. D. Hancock, S. M. Dobson, A. Evers, P. W. Wade, M. P. Ngwenya, J. C. A. Boeyens and K. P. Wainwright, *J. Am. Chem. Soc.*, 1988, **110**, 2788, and refs. therein.
5 K. Henrick, P. A. Tasker and L. F. Lindoy, *Prog. Inorg. Chem.*, 1985, **33**, 1.
6 K. Henrick, L. F. Lindoy, M. McPartlin, P. A. Tasker and M. P. Wood, *J. Am. Chem. Soc.*, 1984, **106**, 1641; H, J. Goodwin, K. Henrick, L. F. Lindoy, M. McPartlin and P. A. Tasker, *Inorg. Chem.*, 1982, **21**, 3923.
7 R. Das and K. Nag, *Inorg. Chem.*, 1991, **30**, 2831.
8 K. K. Nanda, R. Das, M. J. Newlands, R. Hynes, E. J. Gabe and K. Nag, *J. Chem. Soc., Dalton Trans.*, 1992, 897.
9 R. Das, K. K. Nanda, K. Venkatsubramanian, P. Paul and K. Nag, *J. Chem. Soc., Dalton Trans.*, 1992, 1253.
10 M. D. Glick, R. L. Lintvedt, T. J. Anderson and J. L. Mack, *Inorg. Chem.*, 1976, **15**, 2258.
11 A. B. P. Lever, *Inorganic Electronic Spectroscopy*, 2nd edn., Elsevier, Amsterdam, 1984.
12 L. Fabrizzi, *Inorg. Chem.*, 1977, **16**, 2667.
13 F. L. Urbach, in *Coordination Chemistry of Macrocyclic Compounds*, ed. G. A. Melson, Plenum, New York, 1979, p. 345.
14 J. S. Coleman, L. P. Varga and S. H. Mastin, *Inorg. Chem.*, 1970, **9**, 1015.
15 K. L. Brown, *Inorg. Chim. Acta*, 1979, **37**, L513.
16 A. J. Bard and L. R. Faulkner, *Electrochemical Methods*, Wiley, New York, 1980, p. 488.
17 F. Ullman and K. Brittner, *Chem. Ber.*, 1909, **42**, 2539.
18 S. K. Mandal, L. K. Thompson, K. Nag, J. P. Charland and E. J. Gabe, *Inorg. Chem.*, 1987, **26**, 1391.
19 A. C. T. North, D. C. Phillips and F. S. Mathews, *Acta Crystallogr., Sect. A*, 1968, **24**, 351.
20 P. Main, G. Germain, J. P. Declercq and M. M. Woolfson, MULTAN 82, A System of Computer Programs for the Automatic Solution of Crystal Structures from X-Ray Data, University of York, 1982.
21 J. D. Dunitz and P. Seiler, *Acta Crystallogr., Sect. B*, 1973, **29**, 589.
22 *International Tables for X-Ray Crystallography*, Kynoch Press, Birmingham, 1974, vol. 4.
23 Enraf-Nonius Structure Determination Package, Enraf-Nonius, Delft, 1985.
24 C. K. Johnson, ORTEP II, Program for Thermal Ellipsoid Plotting, ORNL, Oak Ridge, TN, 1976.

Received 31*st December* 1992; *Paper* 2/06924E